INTERNATIONAL JOURNAL FOR NUMERICAL METHODS IN FLUIDS
Int. J. Numer. Meth. Fluids 2001; **37**: 45–64 (DOI: 10.1002/fld.164)

Boundary element analysis of driven cavity flow for low and moderate Reynolds numbers

M. Aydin[1] and R. T. Fenner*,[2]

Department of Mechanical Engineering, Imperial College, London, U.K.

SUMMARY

A boundary element method for steady two-dimensional low-to-moderate-Reynolds number flows of incompressible fluids, using primitive variables, is presented. The velocity gradients in the Navier–Stokes equations are evaluated using the alternatives of upwind and central finite difference approximations, and derivatives of finite element shape functions. A direct iterative scheme is used to cope with the non-linear character of the integral equations. In order to achieve convergence, an underrelaxation technique is employed at relatively high Reynolds numbers. Driven cavity flow in a square domain is considered to validate the proposed method by comparison with other published data. Copyright © 2001 John Wiley & Sons, Ltd.

KEY WORDS: boundary element method; driven cavity flow; Navier–Stokes equations; viscous flows

1. INTRODUCTION

In the literature many computational methods are proposed for solving the Navier–Stokes equations of viscous flow, and among them finite difference (FDM), finite volume (FVM) and finite element methods (FEM) are well established. Although the boundary element method (BEM) is firmly established for the solution of potential flow problems, applications to viscous flow problems have only recently been explored. The main advantage of the boundary element method is that only the boundary needs to be discretized for potential flow problems. Thus, the calculation domain is reduced by one dimension. However, BEM loses its appeal somewhat for viscous flows since the inclusion of the inertial terms of the Navier–Stokes equations complicates the problem considerably. This makes the equations non-linear and requires

* Correspondence to: Department of Mechanical Engineering, Imperial College of Science, Technology and Medicine, Exhibition Road, London, SW7 2BX, U.K. Tel.: +44 020 75947060; fax: +44 020 78238845.
[1] Current address: Institute for Nuclear Energy, Istanbul Technical University, Ayazaga Campus, Maslak 80626, Istanbul, Turkey.
[2] E-mail: r.fenner@ic.ac.uk

Received January 2000
Revised July 2000

discretization of the domain. Recently, a substantial amount of research has been directed to solving the Navier–Stokes equations with BEM.

The integral equations and fundamental solutions for Stokes flow presented by Oseen [1] can be considered as a first step in the BEM analysis of fluid flow. Later the fundamental solutions were called Stokeslet [2]. The BEM solution of the Navier–Stokes equations was first formulated in terms of vorticity and velocity by Wu *et al*. [3]. Mass and momentum conservation equations are partitioned into their kinematic and kinetic parts in this technique. The kinetic part is described by the non-linear vorticity transport equation, whereas the kinematic one, which is governed by a Poisson equation, determines the velocity field from a known vorticity field. Later, a vorticity–streamfunction integral approach was developed by Onishi *et al*. [4]. These vorticity related formulations have the main advantages of eliminating pressure from the solution procedure and satisfying continuity automatically. They are also advantageous when applied to two-dimensional flows, due to involving fewer unknowns. However, the extension to three dimensions is less attractive. This is due to the fact that vorticity is no longer a scalar, and there is a total of six degrees of freedom at each node [5]. These formulations are not generally applicable since boundary conditions in terms of vorticity, streamfunction and their normal derivatives will rarely be known. Further, they require an iterative procedure even for Stokes flow [6].

The first boundary element treatment using primitive variables (pressure and velocity) was used for steady Stokes flow past arbitrary objects [7]. Later, the analysis was extended to solve the full Navier–Stokes steady flow equations by including non-linear terms in two-dimensional BEM analysis [8]. In this work, a finite element approximation was chosen to evaluate the velocity gradients within the flow. Constant surface elements were used at the boundary and three-noded linear internal cells were utilized throughout the domain of interest, and solutions were obtained at low Reynolds numbers. The same analysis was enhanced with a boundary element representation of Oseen's linearized equations for plane flow past a cylinder of arbitrary cross-section [9]. However, solutions could not be obtained beyond a Reynolds number of 1.0.

A new integral formulation with primitive variables, mainly based on Bush and Tanner's implementation, was proposed by incorporating linear boundary elements [10]. Hormander's method in the theory of partial differential equations was adopted to construct the fundamental solution. Two-dimensional cavity flow was solved to validate the analysis. However, nothing was mentioned about the numerical implementation.

Since the BEM has been successfully applied in the field of stress analysis, BEM researchers have utilized the analogy between Navier's equations of elasticity and the penalty function formulation of viscous incompressible fluids to solve flow problems. The evaluation of the convective terms in the Navier–Stokes equations was investigated in the penalty function formulation [11,12]. However, inserting a penalty parameter into the continuity equation implies an artificial compressibility of the flow.

Recently, the divergence theorem has been applied to the non-linear convective volume integral term, together with the free stream velocity concept being used to concentrate the non-linear effects in the vicinity of the boundaries [13]. Although the application of the divergence theorem to the convective term eliminates the requirement for computation of interior derivatives, domain discretization is still needed. However, the formulation using FEM

based derivatives (the present one) is less expensive than the divergence theorem formulation. This is due to the fact that convective terms evaluated using FEM derivatives have fewer kernel terms involved than the divergence theorem formulation, and less severe singularity in the kernel [14]. It was also concluded that the successive substitution iterative method fails to converge beyond $Re = 100$.

The dual reciprocity method (DRM) has also been used, to transform the non-linear convective volume integral term to boundary integrals [15]. The formulation was tested with the case of steady flow inside a closed circular cylindrical container. It was reported that convergence problems occurred for Reynolds number 32 and showed results up to $Re = 100$. Later, an indirect BEM with DRM was applied for three-dimensional solution of driven cavity flow [16]. The indirect formulation reduced computing time and the solutions were given for $Re = 100$.

The penalty function technique with the Oseen fundamental solution has been employed for steady viscous flows [17]. It was suggested that fundamental solutions for viscous flows that take the convective nature of the flow into consideration are necessary for solutions of viscous flows at high Reynolds numbers. Driven cavity flow problems were solved, but the algorithm failed to capture the secondary vortices at the corners, and results were limited to Reynolds number up to 1000. Recently, Grigoriev and Dargush [18] improved the penalty function formulation employing hexagonal subregions and discretized the integral equation for each subregion. Such a method is more akin to a FEM, but with an integral equation treatment for each subregion. They solved the same problem with a non-uniform mesh of 1680 hexagonal subregions (each made up of three quadrilateral cells) and were able to capture the secondary vortices and obtained convergent results up to $Re = 5000$.

A three-dimensional BEM was developed for Stokes flow in transient state[19]. Mixing flows of Newtonian and viscoelastic fluids were considered in multiply connected moving domains.

More recently, Power and Mingo [20] enhanced the DRM formulation with a subdomain decomposition approach in order to cope with higher Reynolds number flows. They tested the formulation with the cases of driven cavity flow and backward facing step problems. They were able to get convergent solutions of driven cavity flow up to $Re = 600$ with 25 non-uniform square subdomains.

In the present paper, a primitive variable formulation is used along with Stokes' fundamental solution. The non-linear terms are considered as pseudo-body forces in the boundary integral equation and the convective terms are treated using finite difference schemes and derivatives of finite element shape functions. The body terms are evaluated by direct iteration based on successive substitutions of the updated velocity field. In order to achieve convergence at relatively high Reynolds numbers, an accurate integration scheme with higher order domain cells and an underrelaxation technique is employed. The well-known benchmark problem of driven-cavity flow in a square domain is considered to validate the proposed method.

2. BOUNDARY INTEGRAL EQUATION

The boundary integral equation form of the governing equations for an incompressible fluid together with traction and velocity boundary conditions over the fluid boundaries, is written as follows [8]

$$C_{ij}u_j(P) = \rho \int_\Omega (f_j(Q) - a_j(Q))u^*_{ij}(P, Q)\,\mathrm{d}\Omega + \int_\Gamma t_j(Q)u^*_{ij}(P, Q)\,\mathrm{d}\Gamma - \int_\Gamma u_j(Q)t^*_{ij}(P, Q)\,\mathrm{d}\Gamma \tag{1}$$

where t_j, u_i are the traction and velocity vectors respectively, ρ is the fluid density, f_j are arbitrary body forces, a_j are the acceleration components, P and Q are source and field points respectively. The a_j convective term is given by

$$a_j = u_k \frac{\partial u_j}{\partial x_k} \tag{2}$$

The Stokeslet fundamental solution in two dimensions is written in the following form:

$$u^*_{ij}(P, Q) = \frac{1}{4\pi\mu}\left\{-\ln(r)\delta_{ij} + \frac{\partial r}{\partial x_i}\frac{\partial r}{\partial x_j}\right\} \tag{3}$$

$$t^*_{ij}(P, Q) = -\frac{1}{\pi r}\left\{\frac{\partial r}{\partial n}\frac{\partial r}{\partial x_i}\frac{\partial r}{\partial x_j}\right\} \tag{4}$$

where r is the distance between P and Q, and n is the unit outward normal vector.

The boundary is represented with three-noded straight or curved isoparametric elements, which use quadratic variation for both geometry and variables. The Cartesian co-ordinates $x_i(\xi)$ of an arbitrary point of an element defined in terms of nodal co-ordinates x_i^c and shape functions can be calculated from

$$x_i(\xi) = N^c(\xi)x_i^c \tag{5}$$

where ξ is the local intrinsic co-ordinate, which has its origin at the midpoint node and values -1 and $+1$ at the end nodes, N^c are the shape functions of the isoparametric boundary elements, c is the node number which ranges from 1 to 3, and $i = 1, 2$. Each of the solution variables, tractions t_i and velocities u_i, can then be represented in terms of the same shape functions as follows:

$$u_i(\xi) = N^c(\xi)u_i^c$$

$$t_i(\xi) = N^c(\xi)t_i^c \tag{6}$$

where u_i^c and t_i^c are the nodal values of velocity and traction respectively.

In addition to the boundary discretization, the domain must be discretized into cells. The Cartesian co-ordinates $x_i(\xi_1, \xi_2)$ of an arbitrary point of a quadrilateral cell defined in terms of nodal co-ordinates x_i^c and shape functions can be calculated from

$$x_i(\xi_1, \xi_2) = \sum_c x_i^c L^c(\xi_1, \xi_2) \tag{7}$$

where the shape functions of the cell, $L^c(\xi_1, \xi_2)$, are functions of intrinsic co-ordinates ξ_1 and ξ_2, which have their origin at the centre of the cell and values -1 and $+1$ at the edges of the cell. The variation of the velocity field at any point of a cell can similarly be written as

$$u_i(\xi_1, \xi_2) = \sum_c u_i^c L^c(\xi_1, \xi_2) \tag{8}$$

where u_i^c are the nodal velocities.

Let the boundary Γ and the domain Ω be represented by M isoparametric quadratic boundary elements and N quadratic quadrilateral cells respectively. Substituting the parametric representations of geometry, velocity and traction into Equation (1), the boundary integral equation may then be written in discretized form as

$$\begin{aligned} C_{ij}u_j(P) + \sum_{m=1}^{M}\sum_{c=1}^{3} u_j(Q) \int_{-1}^{+1} t_{ij}^*(P, Q)N^c(\xi)|J_\Gamma(\xi)|\,\mathrm{d}\xi \\ = \sum_{m=1}^{M}\sum_{c=1}^{3} t_j(Q) \int_{-1}^{+1} u_{ij}^*(P, Q)N^c(\xi)|J_\Gamma(\xi)|\,\mathrm{d}\xi \\ + \sum_{n=1}^{N}\sum_{k=1}^{K} \int_{-1}^{+1}\int_{-1}^{+1} b_j(Q)u_{ij}^*(P, Q)L^k(\xi_1, \xi_2)|J_\Omega(\xi_1, \xi_2)|\,\mathrm{d}\xi_1\,\mathrm{d}\xi_2 \end{aligned} \tag{9}$$

where $b_j(Q) = f_j(Q) - a_j(Q)$ is the total body force, k takes values from 1 to 8 (the nodes of an internal cell). The Jacobian of boundary transformation from global to intrinsic co-ordinate ξ, is $J_\Gamma(\xi) = \mathrm{d}\Gamma/\mathrm{d}\xi$, and the Jacobian of domain transformation from the global to the intrinsic co-ordinate system, ξ_1 and ξ_2, is $J_\Omega(\xi_1, \xi_2) = \partial\Omega/\partial(\xi_1, \xi_2)$.

3. CONVECTIVE TERMS

3.1. Central difference scheme

The convective terms are considered as pseudo-body forces and treated using finite difference schemes. The convective terms are approximated by assigning a constant value of the gradient to each cell. Using the usual notation of computational fluid dynamic (CFD) methods, the centre point of the cell of interest is identified by P and its neighbours the nodes to the west, east, north and south are identified by W, E, N and S respectively. The distances between the nodes are identified similarly, for example the distance between the nodes E and W is denoted by EW. The convective term components given in Equation (2) can be written

$$a_j = u_1^P\left\{\frac{u_j^E - u_j^W}{EW}\right\} + u_2^P\left\{\frac{u_j^N - u_j^S}{NS}\right\} \tag{10}$$

3.2. Upwind scheme

In the central finite difference scheme, convection is equally dependent upon both upstream and downstream velocities. If it is assumed that the convection of the cell is received from upstream and transmitted to the downstream, taking the convection contribution only from the upstream direction is called upwind differencing

$$a_j = u_1^p \begin{cases} (u_j^p - u_j^W)/PW & u_1^p \geq 0 \\ (u_j^E - u_j^p)/EP & u_1^p < 0 \end{cases} + u_2^p \begin{cases} (u_j^p - u_j^S)/PS & u_2^p \geq 0 \\ (u_j^N - u_j^p)/NP & u_2^p < 0 \end{cases} \tag{11}$$

3.3. Derivatives of finite element shape functions

The velocity gradients at any location can also be obtained by differentiating shape functions of the relevant cell. Recalling the variation of the velocity field in the cell $u_i(\xi_1, \xi_2) = \Sigma_c\, u_i^c L^c(\xi_1, \xi_2)$, the velocity gradient can then be written in the form

$$\frac{\partial u_i(\xi_1, \xi_2)}{\partial x_j} = \sum_c u_i^c \frac{\partial L^c(\xi_1, \xi_2)}{\partial x_j} \tag{12}$$

where u_i^c are the nodal velocities and $i = 1, 2$. Substituting Equation (12) into the Equation (2), the convective terms are obtained as

$$a_j(\xi_1, \xi_2) = \sum_m \sum_c u_k^m L^m(\xi_1, \xi_2) u_j^c \frac{\partial L^c(\xi_1, \xi_2)}{\partial x_k} \tag{13}$$

where $j = 1, 2$, and m ranges from 1 to 8, and the derivatives of shape functions with respect to global co-ordinates $\partial L^c(\xi_1, \xi_2)/\partial x_k$ may be found from

$$\begin{bmatrix} \dfrac{\partial L^c(\xi_1, \xi_2)}{\partial x_1} \\ \dfrac{\partial L^c(\xi_1, \xi_2)}{\partial x_2} \end{bmatrix} = [J_\Omega(\xi_1, \xi_2)]^{-1} \begin{bmatrix} \dfrac{\partial L^c(\xi_1, \xi_2)}{\partial \xi_1} \\ \dfrac{\partial L^c(\xi_1, \xi_2)}{\partial \xi_2} \end{bmatrix} \tag{14}$$

where $[J_\Omega(\xi_1, \xi_2)]^{-1}$ is the inverse of the Jacobian $J_\Omega(\xi_1, \xi_2)$, so that $[J_\Omega(\xi_1, \xi_2)]^{-1}$ is of the form

$$[J_\Omega(\xi_1, \xi_2)]^{-1} = \begin{bmatrix} j_{11} & j_{12} \\ j_{21} & j_{22} \end{bmatrix} \tag{15}$$

On combining Equations (13) and (15), the convective term $a_j(\xi_1, \xi_2)$ in unabridged notation may be written as

$$a_1(\xi_1, \xi_2) = \sum_m \sum_c u_1^m L^m(\xi_1, \xi_2) u_1^c \left\{ j_{11} \frac{\partial L^c(\xi_1, \xi_2)}{\partial \xi_1} + j_{12} \frac{\partial L^c(\xi_1, \xi_2)}{\partial \xi_2} \right\} + \sum_m \sum_c u_2^m L^m(\xi_1, \xi_2) u_1^c \left\{ j_{21} \frac{\partial L^c(\xi_1, \xi_2)}{\partial \xi_1} + j_{22} \frac{\partial L^c(\xi_1, \xi_2)}{\partial \xi_2} \right\} \tag{16}$$

$$a_2(\xi_1, \xi_2) = \sum_m \sum_c u_1^m L^m(\xi_1, \xi_2) u_2^c \left\{ j_{11} \frac{\partial L^c(\xi_1, \xi_2)}{\partial \xi_1} + j_{12} \frac{\partial L^c(\xi_1, \xi_2)}{\partial \xi_2} \right\} + \sum_m \sum_c u_2^m L^m(\xi_1, \xi_2) u_2^c \left\{ j_{21} \frac{\partial L^c(\xi_1, \xi_2)}{\partial \xi_1} + j_{22} \frac{\partial L^c(\xi_1, \xi_2)}{\partial \xi_2} \right\} \tag{17}$$

4. INTEGRATION

The accuracy of the boundary element method essentially depends on the accuracy of evaluation of integrals. The details of the integration schemes for Equation (9) are covered in Aydin [21]. They are summarized here.

4.1. Boundary integrals

The integrals of kernel and shape function products can be evaluated depending on the position of the load point P with respect to the boundary element over which the integrations are carried out. When a load point P is outside the element, both kernels are non-singular, with finite values within the integration region, and standard Gaussian quadrature is employed.

When P and Q are in the same element but do not coincide, although $u_{ij}^*(P, Q)$ and $t_{ij}^*(P, Q)$ are both singular (because they contain terms of the order of $\ln(1/r)$ and $1/r$ respectively) the shape function $N^c(\xi)$ in the vicinity of P is of order r. The integrals are evaluated using standard Gaussian quadrature.

When P and Q coincide, $N^c(\xi)$ equals unity and both kernels contain singular terms, and standard Gaussian quadrature can no longer be used. The kernel $u_{ij}^*(P, Q)$ requires special treatment to deal with the $\ln(1/r)$ singularity, and logarithmic Gaussian quadrature is used. On the other hand, there is no quadrature formula suitable for the kernel $t_{ij}^*(P, Q)$. Besides, calculation of the parameter $C_{ij}(P)$ is also needed. This is done by applying the boundary integral equation to a problem which will result in a simple solution. For this purpose, a case equivalent to rigid body motion in elastostatic problems [22] is considered: namely, constant unit velocity in both directions for all nodes corresponds to zero tractions everywhere.

4.2. Domain integration

When the source point P is located outside the element to be integrated over, the domain integration appearing in Equation (9) has no singularity. Therefore, standard Gaussian quadrature is used. When the source point P is a node of the element to be integrated over, the kernel $u_{ij}^*(P, Q)$ becomes singular as the distance r approaches zero. For constant convective cells, the integration is performed analytically. For quadratic cells, the integration scheme adopted here is based on the work by Lachat and Watson [23]. The latter was adopted

by Tan and Fenner [24] for three-dimensional stress analysis of cracked components and Ghaderi-Panah and Fenner [25] for contact problems. The basic idea behind the technique is to transform the integration into new co-ordinates, such that the Jacobian of the transformation is small near the source point. Thus, singular behaviour of the kernel is moderated by the small Jacobian. Standard Gaussian quadrature is then applied to each subcell.

5. SOLUTION PROCEDURE

After calculating integrals and applying boundary conditions, Equation (9) can be rearranged in matrix–vector form as [26]

$$[A][x]^{k+1} = [y] + [b]^{k} \tag{18}$$

where $[A]$ is the resulting matrix of coefficients, $[y]$ is a known vector, $[x]$ represents the unknown boundary values, and $[b]$ is a vector corresponding to body force terms. Here the superscripts k and $k+1$ indicate the k and $k+1$ iterations of the predicted solutions respectively. Once the boundary solution is obtained, the interior velocity field can be found as

$$[v]^{k+1} = [H][t]^{k+1} - [G][u]^{k+1} + [c]^{k} \tag{19}$$

where $[v]$ is a vector representing the internal solutions, $[t]$ and $[u]$ are the boundary vectors of traction and velocity, $[H]$ and $[G]$ are coefficient matrices and $[c]$ is the vector of non-linear terms. To find the solution to the problem, $[b]$ and $[c]$ are set to zero as initial estimates, which corresponds to Stokes flow. The relaxation scheme, for example for the boundary unknowns, $[x]$, is written as follows

$$[x] = \beta[x]^{k} + (1-\beta)[x]^{k-1} \tag{20}$$

where $[x]^{k}$ and $[x]^{k-1}$ are the values predicted in iterations k and $k-1$ respectively, and $[x]$ is the value of the vector used to evaluate the vector $[b]$ for the next iteration. The same relaxation scheme is applied to the internal solutions in each iteration until the desired convergence is obtained. The relaxation parameter β varies between 0 and 1. When the residuals are smaller than a certain tolerance ε, the results are considered converged. The convergence tolerance ε is very small and usually in the range of 10^{-4}–10^{-6}.

6. NUMERICAL RESULTS

Driven cavity flow is strongly non-linear for high Reynolds number. It has been extensively studied with all numerical methods for viscous flows and has become a benchmark problem in the literature. In the BEM literature, Tosaka *et al.* [10] solved the case using primitive variables. They used a fine mesh of 82 linear boundary elements and 840 linear triangular

interior cells. However, results were given only for $Re = 100$. Nothing was mentioned about the position of the vortex centre and the existence of secondary vortices at the corners.

Kitagawa *et al.* [11] used a BEM with a penalty function formulation to solve this problem. They used a non-uniform mesh of 160 linear boundary elements and 157 rectangular constant interior cells. They reported that at $Re = 400$, the successive substitution iterative algorithm (direct iteration) was convergent for the upwind finite difference scheme but produced different results from those published in the literature. In the case of central differences, the iteration cycle was unstable and not convergent [11,12]. Again, nothing was mentioned about the location of the vortex centre and capturing the secondary vortices at the corners.

Dargush and Banerjee [13] solved the problem with a non-uniform mesh of 324 quadratic domain cells and showed results up to $Re = 1000$. It was reported that the successive substitution iterative algorithm failed to converge beyond $Re = 100$. Beyond that range the use of a Newton–Raphson type algorithm was imperative [13].

Grigoriev and Fafurin [17] presented a BEM solution using the penalty function technique and the Oseen fundamental solution for driven cavity flow. Results were presented for a non-uniform mesh with 324 quadratic interior cells. They reported that their algorithm failed to capture the secondary vortices at the corners. However, in a recent paper, Grigoriev and Dargush [18] improved the penalty function formulation employing hexagonal subregions and discretized the integral equation for each subregion as in FEM. They solved the same problem with a non-uniform and much refined mesh of 5040 quadrilateral cells and were able to capture the secondary vortices and obtained convergent results of up to $Re = 5000$.

Driven cavity flow is defined as steady laminar incompressible flow in a unit square cavity whose top wall moves with constant velocity in the plane of the cavity cross section. Therefore, the flow movement inside the cavity is induced by the top wall of the cavity. The fluid velocities on the left, right and bottom sides are fixed at zero in both directions, while a uniform non-zero velocity is along the top wall as boundary conditions.

The boundary of the problem is uniformly discretized for Stokes flow using a mesh with 40 boundary elements. The works of Burggraf [27], and Karaeorghis *et al.* [28] are used to assess the horizontal velocity results along the vertical centre line of the cavity of the present work. They are all plotted in Figure 1. The finite difference method was used with a 1024 node grid by Burggraf [27], employing the vorticity–streamfunction approach. The indirect boundary element method was adopted to obtain the results iteratively in the work of Karaeorghis *et al.* [28]. Only half of the cavity was taken as the solution domain, with 136 nodes. All results agree well with one another, as well as with the present solutions, indicating that for $Re = 0$, the coarse mesh employed here is adequate.

Checking bulk continuity in CFD is important for an overall quantitative sense of the solution accuracy. This comparison is done for both the u_1 and u_2 components of velocity. Velocity profiles for the u_1 component along the vertical line and the u_2 component along the horizontal line, both passing through the geometric centre of the cavity, are considered to calculate volumetric flow rates, Q. Integration of the velocity profile over these sections should result in $Q = 0$ for both directions. Convergence of the obtained results to $Q = 0$ is tested for a number of uniform meshes. Integrations to calculate the volumetric rates are performed by using Simpson's rule. Table I lists the calculated numerical values of the volumetric flow rates corresponding to the velocity profiles for different numbers of boundary elements. These

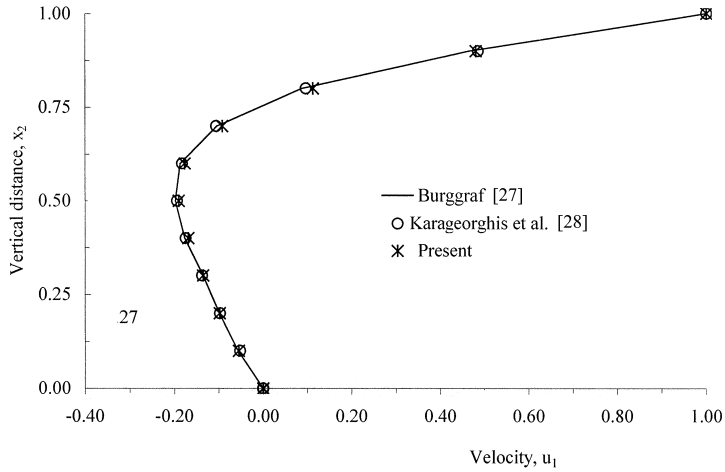

Figure 1. Velocity profile on vertical centre line of the driven cavity for $Re = 0$.

Table I. Volumetric flow rates through geometric centre of the cavity for $Re = 0$.

Volumetric flow rates	16 elements	32 elements	64 elements	80 elements
$Q_1 = \int u_1 \, dx_2/Q_c$	0.058	0.029	0.015	0.012
$Q_2 = \int u_2 \, dx_1/Q_c$	−0.039	−0.019	−0.009	−0.007

values are divided by characteristic flow rate, Q_c, which is the horizontal rate that would occur in the absence of the side walls (linear velocity profile in the vertical direction), to help quantify the errors.

As finer meshes are used, volumetric flow rates converge to zero for both directions of flow. From the table, Q_1 has positive values indicating that there is a net flow in the positive (horizontal) x_1 direction, whereas negative Q_2 implies a net flow in the negative (vertical) direction of x_2.

The problem for finite Reynolds number flow is solved using constant interior cells with both the upwind and central difference approaches, and quadratic interior cells with derivatives of finite element shape functions. Table II documents the characteristics of the uniform meshes of quadratic interior cells. The only difference between the constant cell meshes and the quadratic ones is that there are more internal nodes used in constant cell meshes, whereas the other characteristics remain the same. For constant cell meshes, there are 40 internal nodes used in Mesh 1, 176 in Mesh 2 and 736 in Mesh 3. The problem is first discretized using Mesh 1 with constant cells to obtain the solution at $Re = 10$. Convergence occurs after five iterations for both schemes. The results obtained for both finite difference schemes are compared with FEM results [29], as shown in Figure 2. A fine mesh with 16 nodes along the vertical line

Table II. Meshes for driven cavity flow.

	No. of boundary elements	No. of internal nodes	No. of cells
Mesh 1	16	33	16
Mesh 2	32	161	64
Mesh 3	64	705	256
Mesh 4	80	1121	400

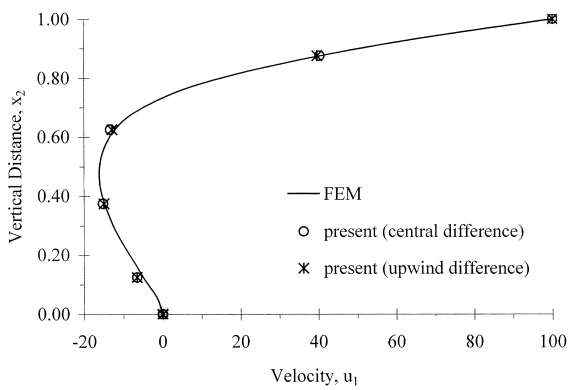

Figure 2. u_1-velocity profile along vertical line through geometric centre for $Re = 10$.

through the centre of the cavity and the penalty function approach were used in this FEM work. The present algorithm with the upwind scheme for this mesh fails to converge at $Re = 40$, whereas the one using central differences continues to converge up to $Re = 100$.

Meshes 1–3 are all used for $Re = 100$, for which many results are available in the literature. The results are plotted with the finite difference solutions [24,27] in Figure 3. Ghia *et al.* [30] used a very fine uniform grid with 129×129 points to analyse the case at $Re = 100$. They represented the governing equations in terms of streamfunction and vorticity parameters. The discretization was performed with central differences, while the convective terms were represented with the upwind scheme. As shown in Figure 3(a), although all results converge for the published FDM solutions with the refined meshes employed, the best agreement between FDM and the present solutions are obtained with quadratic Mesh 3, indicating the importance of the mesh. The same observations can be made for the u_2 profile along the horizontal line through the geometric centre in Figure 3(b). Nevertheless, the present results with the upwind scheme offer slightly different effects compared to the others, which confirm the observations of Kitagawa [12]. However, convergence difficulties and fluctuations in the solution with this scheme appear even when using Mesh 2. Using the present algorithm with central finite differences, convergent results are obtained up to the limit of $Re = 225$ (relaxation parameter $\beta = 0.2$) for this particular mesh, which conflicts with the observations of Kitagawa [12].

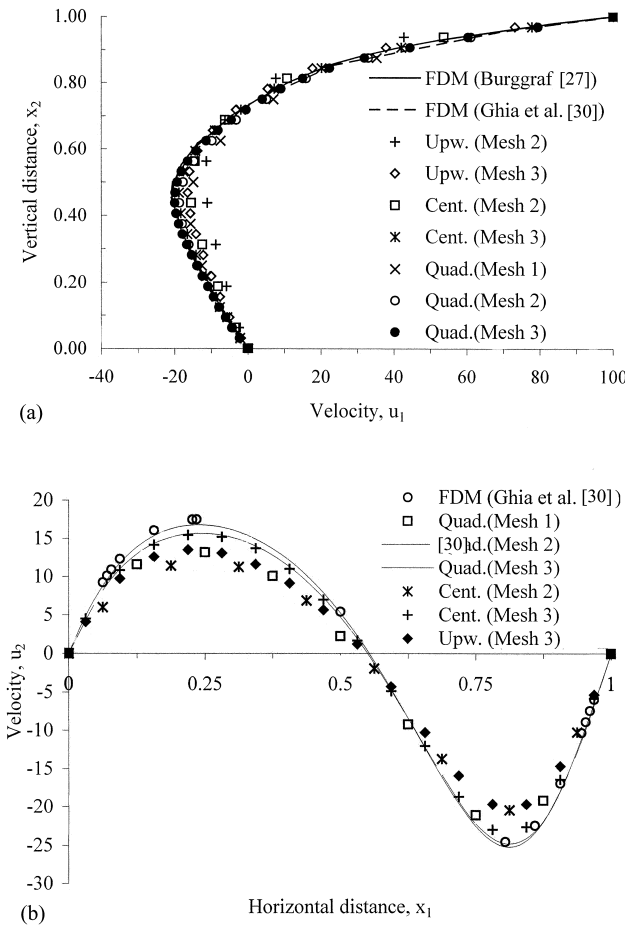

Figure 3. Velocity profile for $Re = 100$: (a) u_1 along vertical line through geometric centre; (b) u_2 along horizontal line through geometric centre.

The u_1 profile results along the vertical line through the geometric centre for $Re = 400$ are compared with the finite difference solutions [30] and also those of Agarwal [31], who used a 121×121 uniform grid with a high order FDM upwind scheme. This comparison is shown in Figure 4(a). Results for u_2-velocity profiles along x_1 through the geometric centre are plotted in Figure 4(b). The present results converge to the published FDM solutions [30] with the refined meshes employed.

The results for $Re = 1000$ are plotted with those of Tosaka [32], Thomasset [30] and, Nallasamy and Prasad [34] in Figure 5. Tosaka [32] formulated the boundary integral equations with primitive variables and constructed the fundamental solution by adopting Hormander's method. He used a 23×25 non-uniform mesh of linear boundary elements and

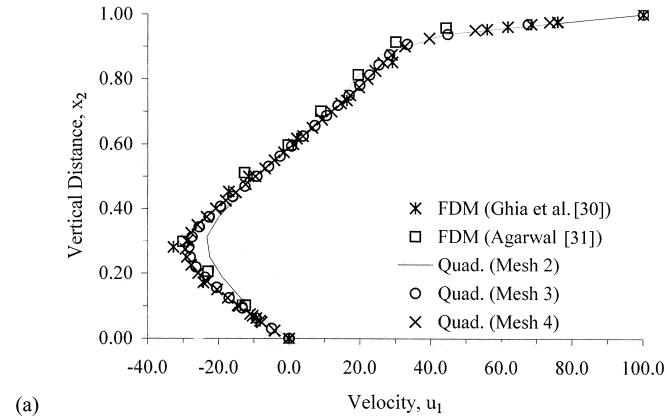

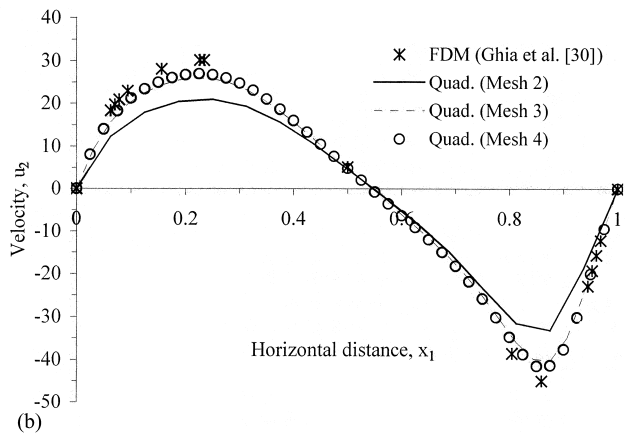

Figure 4. Velocity profile for $Re = 400$: (a) u_1 along vertical line through geometric centre; (b) u_2 along horizontal line through geometric centre.

linear triangular cells to discretize the problem domain. Thomasset [33] used a vorticity–velocity upwind FEM method together with a 12×12 element mesh. Nallasamy and Prasad [34] again used an upwind FEM method. They employed a mesh with 50×50 elements.

Another important way of assessing the results is to compare the positions of the main vortex centre. This is illustrated in Table III. The present results for $Re = 0$ agree with those reported in the works of Gupta and Manohar [35], and Rodriguez-Prada *et al.* [5]. Gupta and Manohar [35] employed a FDM with streamfunction–vorticity. Rodriguez-Prada *et al.* [5] used a BEM and streamfunction–vorticity to solve the case directly without iterations. They used

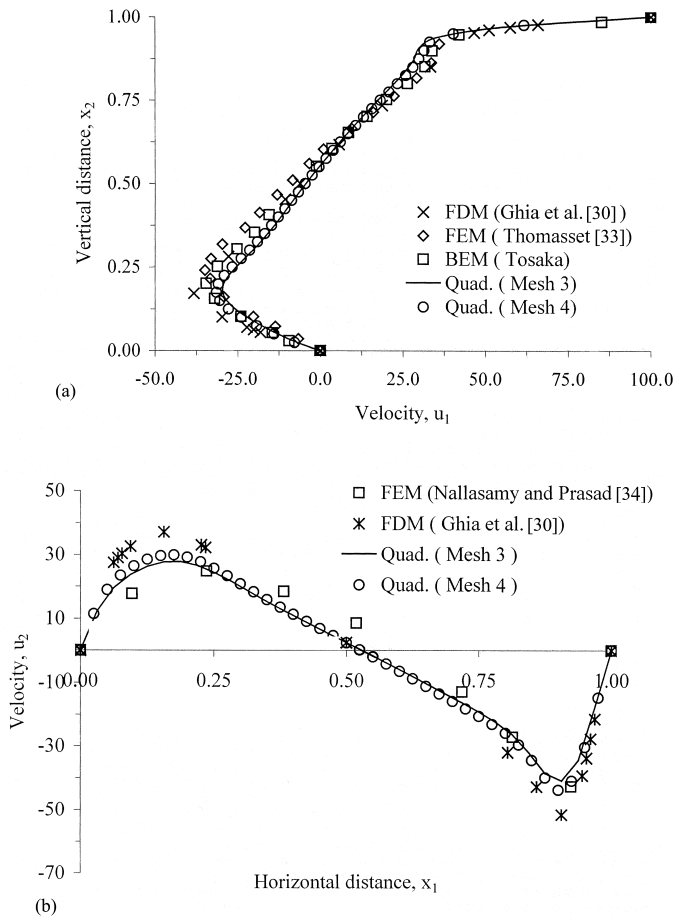

Figure 5. Velocity profile for $Re = 1000$: (a) u_1 along vertical line through geometric centre; (b) u_2 along horizontal line through geometric centre.

a mesh with 64 boundary nodes. The vortex centre moves as the Reynolds number increases, which was described earlier by Burggraf [27]. Present predictions for the vortex centre location are compared with some available data published in the literature. For $Re = 100$, the results are also compared with the experimental ones [36].

The results obtained in terms of a velocity vector field for $Re = 1000$ are given in Figure 6. Magnified views of the secondary vortices at the bottom corners are shown in Figure 7. Although the secondary vortex at the right hand corner can be clearly seen, the centre of the vortex at the left hand corner is close to the bottom boundary and not seen well. A finer mesh at this corner may be used in order to resolve the vortex here. As seen from Figure 6, the

Table III. Comparisons of the main vortex centre location (x_1, x_2) in driven cavity flow.

Studies by	$Re = 0$	$Re = 100$	$Re = 400$	$Re = 1000$
Gupta and Manohar [35]	(0.500, 0.750)	(0.63, 0.75)	—	—
Rodriguez-Prada *et al.* [5]	(0.500, 0.750)	(0.62, 0.75)	—	—
Burggraf [27]	(0.500, 0.760)	(0.625, 0.750)	(0.560, 0.615)	—
Ghia *et al.* [30]	—	(0.6172, 0.7344)	(0.5547, 0.6055)	(0.5313, 0.5625)
Grigoriev and Fafurin [17]	—	(0.610, 0.730)	(0.555, 0.610)	(0.545, 0.575)
Matsumoto and Daiguji [37]	—	—	—	(0.530, 0.564)
Mills [36]	—	(0.62, 0.74)	—	—
Schrieber and Keller [38]	—	(0.6167, 0.742)	—	(0.553, 0.650)
Present	(0.500, 0.750)	(0.625, 0.750)	(0.556, 0.611)	(0.5312, 0.5625)

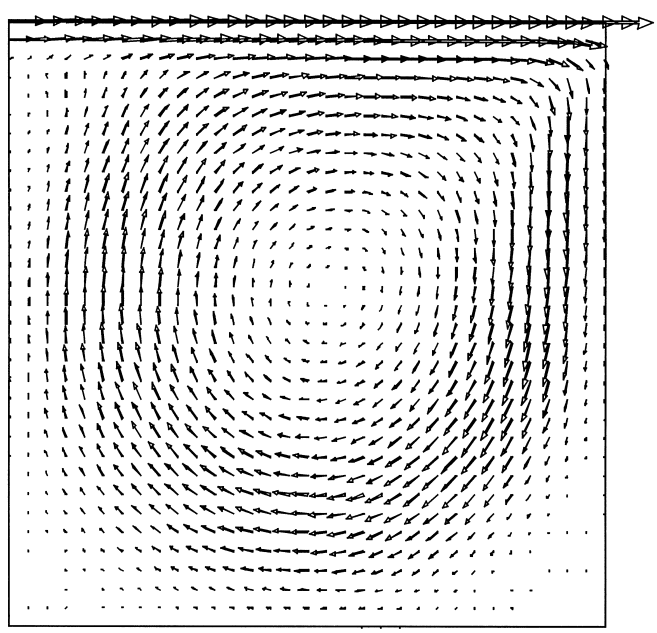

Figure 6. Velocity vectors for $Re = 1000$.

method is also able to sense the existence of another vortex at the left top corner, which is not clear. This is due to the fact that this vortex only becomes really apparent after $Re = 3000$ [30].

Tables IV and V list the calculated numerical values of the volumetric flow rates in two directions for different Reynolds numbers. From Table IV, as Re is increased, the volumetric flow rate increases, indicating that the error increases as well. There is one exception with Mesh 3 for $Re = 1000$. For $Re = 100$ and 400, as finer meshes are used, the volumetric flow rate converges to zero. From Table V, Q_2 has negative values indicating that there is a net flow

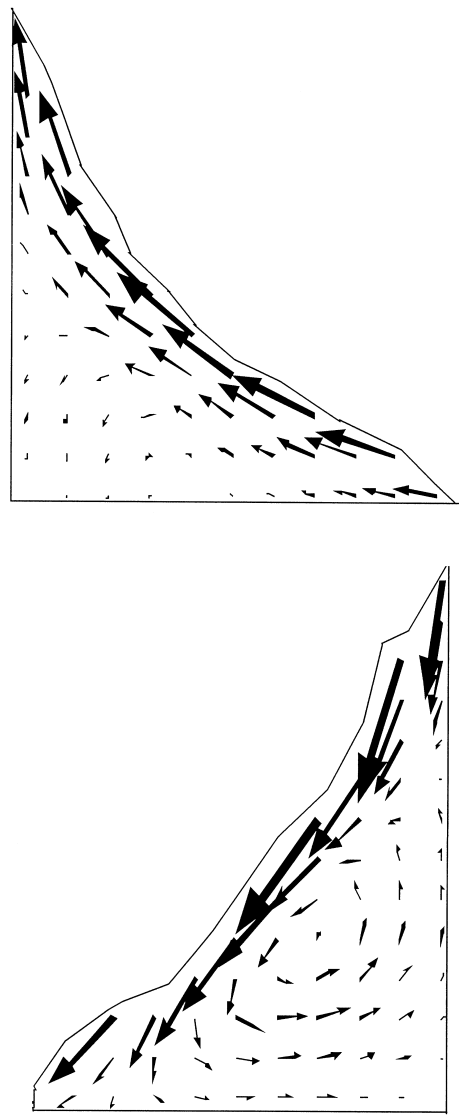

Figure 7. Velocity vectors at the bottom left hand and right hand corners for $Re = 1000$.

in the negative x_2 direction. For $Re = 100$ and 400, as finer meshes are employed, the volumetric flow rate converges to zero. This is valid with Meshes 1 and 2 for $Re = 1000$. However, there is no improvement between Meshes 3 and 4 at this particular Re number.

Table IV. Volumetric flow rate $Q_1 = \int u_1 \, dx_2/Q_c$ through geometric centre of the cavity.

	$Re = 100$	$Re = 400$	$Re = 1000$
Mesh 1	0.0636	0.0777	0.1082
Mesh 2	0.0316	0.0367	0.0433
Mesh 3	0.0156	0.0176	0.0001
Mesh 4	0.0124	0.0139	0.0163

Table V. Volumetric flow rate $Q_2 = \int u_2 \, dx_1/Q_c$ through geometric centre of the cavity.

	$Re = 100$	$Re = 400$	$Re = 1000$
Mesh 1	−0.0318	−0.0155	0.0130
Mesh 2	−0.0167	−0.0099	−0.0017
Mesh 3	−0.0088	−0.0063	−0.0025
Mesh 4	−0.0071	−0.0054	−0.0026

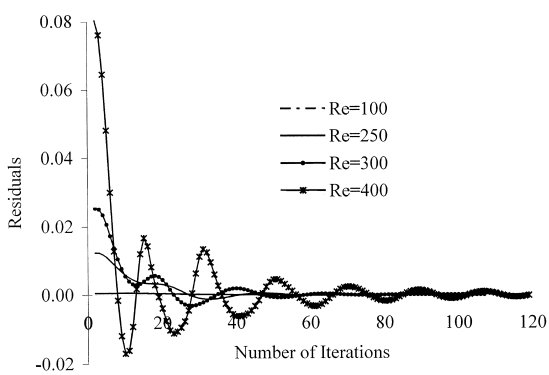

Figure 8. Effect of Reynolds number on convergence ($\beta = 0.08$).

Information about solution parameters such as the number of iterations and relaxation factor hardly appear in the BEM literature. For the purposes of illustration, the effects of *Re* and relaxation factor β on the solution are shown in Figures 8 and 9. At low *Re*, the solution converges more rapidly and monotonically. However, the solution oscillates with larger amplitudes and takes more iterations to achieve convergence when *Re* is increased. Note that setting the underrelaxation factor to the correct value is very important. For this purpose, relaxation factors $\beta = 0.5$, 0.25 and 0.1 are tested. This may be seen in Figure 9, a study which is carried out with Mesh 2 at $Re = 300$. For $\beta = 0.5$, an immediate divergence occurs, whereas for $\beta = 0.25$ the solution oscillates with larger amplitudes and diverges. However, the solution converges uniformly for $\beta = 0.1$.

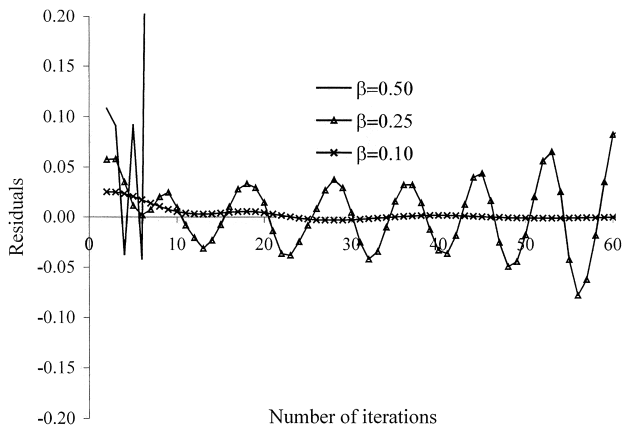

Figure 9. Effect of relaxation factor β on convergence ($Re = 300$, Mesh 2).

Although convergence is obtained for $Re = 1200$ with Mesh 4, at this Reynolds number the solution exhibits what is probably incorrect behaviour. In terms of Reynolds number, this may be a limitation on the present algorithm or a finer mesh may be required to obtain correct solutions at higher Re.

7. CONCLUSIONS

This work presents an accurate and general BEM formulation which was successfully applied to driven cavity flows from zero to moderate Reynolds number conditions.

In the literature, a penalty function is used to enforce the incompressibility constraint in order to obtain accurate BEM solutions [11,12]. However, in this work, it is shown that the penalty function does not have to be applied to the BEM as long as incompressible fundamental solutions (Stokeslet) are used.

To the best of the authors' knowledge, in BEM formulations with primitive variables, the convective terms have not been treated with central and upwind finite difference schemes in the literature. It has been shown that convective terms approximated with these schemes are appropriate for flows at low to medium Reynolds numbers. It was also shown that, under the same conditions, the present algorithm with central finite differences showed a better convergence than the one with the upwind scheme, which conflicts with the observations made for penalty function formulations in the literature [11].

It has also been reported that the successive substitution iterative algorithm is appropriate only for low Reynolds number flows and that it fails to converge for flows beyond this range. When high Reynolds number flows are tackled, the use of a Newton–Raphson type algorithm

was imperative for high Reynolds numbers [13,39]. The present research revealed that this type of algorithm is not necessary as long as an accurate integration scheme with higher order domain cells and an underrelaxation technique are used. The solution interval with the direct iteration algorithm was expanded to cover higher Reynolds number flows as well. It was also noted that setting the underrelaxation factor to the correct value is very important to achieve convergence at higher Reynolds numbers.

Bulk continuity is an important aspect of CFD, which is useful to check. This offers an overall quantitative sense of the solution accuracy. This check seems to have been ignored in the BEM literature, but was used in the current work.

The subject of accuracy is most important for a numerical method. The present BEM formulation produces accurate solutions for both Stokes and finite Reynolds number flows. Detecting the vortex centre of driven cavity flow and resolving vortices at the corners of the cavity were good examples of the accuracy and sensitivity of the present formulation. However, in the BEM literature, either nothing was mentioned about the vortex centre of the driven cavity flow and the secondary vortices at the corners [10–12] or it was reported that the algorithm with the BEM failed to capture the secondary vortices at the corners [17].

Although the present formulation converged for Reynolds numbers larger than 1000, the solution lost its reliability. Therefore, this is the effective Reynolds number limit of the method.

REFERENCES

1. Oseen CW. *Neuere Methoden und Ergebnisse in der Hydrodynamik*. Akademische Verlagsgesellschaft: Leipzig, DDR, 1927.
2. Hancock GJ. The self-propulsion of microscopic organisms through liquids. *Proceedings of the Royal Society*, *A* 1953; **217**(96): 121–143.
3. Wu JC, Thompson JF. Numerical solutions of time-dependent incompressible Navier–Stokes equations using an integro-differential formulation. *Computers in Fluids* 1973; **1**: 197–215.
4. Onishi K, Kuroki T, Tanaka M. An application of boundary element method to incompressible laminar viscous flows. *Engineering Analysis with BEM* 1984; **1**(3): 122–127.
5. Rodriguez-Prada HA, Pironti FF, Saez AE. Fundamental solutions of the streamfunction–vorticity formulation of the Navier–Stokes equations. *International Journal for Numerical Methods in Fluids* 1990; **10**: 1–12.
6. Carneiro HFFM. Fluid flow analysis using the boundary element method. PhD thesis, Cranfield Institute of Technology, 1993.
7. Youngreen GK, Acrivos A. Stokes flow past a particle of arbitrary shape: a numerical method of solution. *Journal of Fluid Mechanics* 1975; **69**(2): 377–403.
8. Bush MB, Tanner RI. Numerical solution of viscous flows using integral equation method. *International Journal for Numerical Methods in Fluids* 1983; **3**: 71–92.
9. Bush MB. Modelling two-dimensional flow past arbitrary cylindrical bodies using boundary element formulations. *Applied Mathematical Modelling* 1983; **7**: 386–394.
10. Tosaka N, Onishi K. Boundary integral equations formulations for steady Navier–Stokes equations using the Stokes fundamental solution. *Engineeining Analysis with BEM* 1985; **2**(3): 128–132.
11. Kitagawa K, Brebbia CA, Wrobel LC, Tanaka M. Boundary element analysis of viscous flow by penalty function formulation. *Engineering Analysis with BEM* 1986; **3**(1): 194–200.
12. Kitagawa K. *Boundary Element Analysis of Viscous Flow*, *Lecture Notes in Engineering*. Springer-Verlag: Berlin, 1990.
13. Dargush GF, Banerjee PK. A boundary element method for steady incompressible thermoviscous flow. *International Journal for Numerical Methods in Engineering* 1991; **31**: 1605–1626.
14. Honkala KA. Boundary element methods for two-dimensional, coupled, thermoviscous flow. PhD thesis, State University of New York, Buffalo, 1992.
15. Power H, Partridge PW. The use of Stokes fundamental solution for the boundary only element formulation of three dimensional Navier–Stokes equations for moderate Reynolds numbers. *International Journal for Numerical Methods in Engineering* 1994; **37**: 1825–1840.

16. Power H, Botte V. An indirect boundary element method for low Reynolds number Navier–Stokes equations in a three-dimensional cavity. *International Journal for Numerical Methods in Engineering* 1998; **41**: 1485–1505.
17. Grigoriev MM, Fafurin AV. A boundary element method for steady viscous fluid flow using penalty function formulation. *International Journal for Numerical Methods in Fluids* 1997; **25**: 907–929.
18. Grigoriev MM, Dargush AV. A poly-region boundary element method for incompressible viscous fluid flows. *International Journal for Numerical Methods in Engineering* 1999; **46**: 1127–1158.
19. Khayat RE, Derdouri A, Frayce D. Boundary element analysis of three-dimensional mixing flow of Newtonian and viscoelastic fluids. *International Journal for Numerical Methods in Fluids* 1998; **28**: 815–840.
20. Power H, Mingo R. The DRM subdomain decomposition approach to solve the two-dimensional Navier–Stokes system of equations. *Engineering Analysis with BEM* 2000; **24**(1): 107–119.
21. Aydin M. *Boundary element analysis of laminar viscous flows*. PhD thesis, Imperial College, London, 1999.
22. Becker AA. *The Boundary Element Method in Engineering—A Complete Course*. McGraw-Hill: New York, 1992.
23. Lachat JC, Watson JO. Effective numerical treatment of boundary integral equation: a formulation for three-dimensional elastostatics. *International Journal for Numerical Methods in Engineering* 1976; **10**: 991–1005.
24. Tan CL, Fenner RT. Three-dimensional stress analysis by the boundary integral equation method. *Journal of Strain Analysis* 1978; **13**: 213–219.
25. Ghaderi-Panah A, Fenner RT. A general boundary element method approach to the solution of three-dimensional frictionless contact problems. *Engineering Analysis with BEM* 1998; **21**: 305–316.
26. Aydin M, Fenner RT, Ghaderi-Panah A. A viscous flow analysis by the boundary element method. In *12th Engineering Mechanics Conference*, *Engineering Mechanics: A Force for the 21st Century*, *17–20* May, San Diego, California, 1998.
27. Burggraf OR. Analytical and numerical studies of the structure of steady separated flows. *Journal of Fluid Mechanics* 1966; **24**(1): 113–151.
28. Karageorghis A, Fairweather G. The simple layer potential method of fundamental solutions for certain biharmonic problems. *International Journal for Numerical Methods in Fluids* 1989; **9**: 1221–1234.
29. Graham FC, Oden JT. *Finite Elements: Fluid Mechanics*, vol. 6. Prentice-Hall: Englewood Cliffs, NJ, 1986.
30. Ghia U, Ghia KN, Shin CT. High-Re solutions for incompressible flow using the Navier–Stokes equations and a multigrid method. *Journal of Computational Physics* 1982; **48**: 387–411.
31. Agarwal RK. A third-order-accurate upwind scheme for Navier–Stokes solutions at high Reynolds numbers. AIAA 81-0112, 1981.
32. Tosaka N. Integral equation method for analysis of Newtonian and non-Newtonian flows. In *Advanced Boundary Element Methods*, Cruse TA (ed.). Springer: Berlin, 1988; 435–442.
33. Thomasset F. *Implementation of Finite Elements Method for Navier–Stokes Equations*. Springer: Berlin, 1981.
34. Nallasamay M, Prasad KK. On cavity flow at high Reynolds numbers. *Journal of Fluid Mechanics* 1977; **79**(2): 391–414.
35. Gupta MM, Manohar RP. Boundary approximations and accuracy in viscous flow computations. *Journal of Computational Physics* 1979; **31**: 265.
36. Mills RD. Experimental investigation on cavity flows. *Journal of Radar and Aeronautics* 1965; **69**: 714.
37. Matumoto Y, Daiguji H. Convective-difference scheme using a general curvilinear coordinate grid for incompressible viscous flow problems. *JSME International Journal Series II* 1992; **35**: 4.
38. Schrieber R, Keller HB. Driven cavity flows by efficient numerical techniques. *Journal of Computational Physics* 1983; **49**: 310–333.
39. Banerjee PK, Honkala KA. Development of BEM for thermoviscous flow. *Computer Methods in Applied Mechanics and Engineering* 1998; **151**: 43–62.

